Research Square

Preprints are preliminary reports that have not undergone peer review.
They should not be considered conclusive, used to inform clinical practice,
or referenced by the media as validated information.

A Simple Model to Predict Complex Coacervation: Forces as Drivers of Phase Change and Structuration

Swapnasopan Datta

sopan.dol@gmail.com

Independent Researcher

Biplab Bawali

Indian Institute of Science Bangalore

Article

Keywords:

Posted Date: October 14th, 2026

DOI: https://doi.org/10.21203/rs.3.rs-11160921/v1

License: This work is licensed under a Creative Commons Attribution 4.0 International License.
Read Full License

Additional Declarations: No competing interests reported.

A Simple Model to Predict Complex Coacervation: Forces as Drivers of Phase Change and Structuration

Swapnasopan Datta[1,*] and Biplab Bawali[2]

[1]Flat 303, Vistas Tower 6, Uniworld City, Newtown AA III B/2, Street 814, Kolkata 700 160, India

[2]Department of Physics, Indian Institute of Science, Bengaluru 560 012, India

Abstract

Biomolecular condensate formation or coacervation has come to the fore as an extremely attractive research area over the past few years, as these condensates have been conjectured to be the most primitive sort of protocells. One of the most studied coacervation processes is the complex coacervation between polyelectrolytes and oppositely charged small molecules. Among these structures, a very well tested system is the poly-L-Lysine/Adenosine Tri Phosphate (pLL/ATP) coacervate. To understand the condensation process, one needs to unravel the forces which dictate the behaviour of pLL dispersed in water at various temperatures and for various monomer charge fractions which are positively charged. Unlike most simulations which have been performed for biologically relevant proteins, here we have used an included solvent Monte Carlo approach on 10-bead flexible strands as the model pLL molecules, where each bead stands for 3 lysine monomers. Initially we have established the 10-bead model for pLL molecules. We have shown that at high pH, when the positive charges are largely neutralized due to deprotonation of the amine groups in the lysine monomers, the strands show a clear tendency to form bundles of rigid and vertically elongated pLL molecules driven by intermolecular attractions caused by hydrophobic repulsion from the aqueous medium. On switching off the hydrophobic interaction, we see no bundle formation and the screened coulomb repulsions dominate pushing the strands away from each other, underscoring the essential role of hydrophobic interaction in pLL structuration. We see a similar tendency to move away from each other by keeping the charges fixed at high reduced temperatures as well. These results agree nicely with experimental observations of the different phases of pLL, in particular the formation of fibrils at high pH and room temperature. Once we established the pLL model, we introduced negatively charged single ATP beads. Based on the screened coulomb attractions between the polymers and the molecules, we could predict the crossover point where the repulsive regime gets converted into an overall attractive one leading to nucleation and growth, resulting into coacervation. We could, therefore, correlate the ATP/pLL ratio to the forces dictating the phase separation process – for the first time to the best of our knowledge. Additionally, we could find the radial charge and ATP and pLL bead density distributions which allows us to understand the internal structures of the condensates.

[1,*]sopan.dol@gmail.com; corresponding author

[2]bbphy_rs@caluniv.ac.in

1. Introduction

Liquid-Liquid Phase Separation (LLPS) has gained considerable interest among chemists and physicists over the past.[1] Coacervates or condensates, which are an outcome of LLPS, are dense droplets consisting of substances which take part in some form of interaction. These macromolecule rich droplets coexist with the relatively dilute solvent, usually under thermodynamic equilibrium. These form spontaneously in aqueous solutions and do not have a 'shell' or a membrane which is why they are often referred to as 'membraneless compartments'.[2,3]

Researchers have proposed that these droplets were primitive cells or 'protocells' initiating the complex process of trapped reaction networks and inter cellular communication, etc. leading to the complicated hierarchy that we call life.[4,5]

Therefore, understanding the specific interactions leading to the formation of such protocells is of paramount importance to complex systems research as it will help the experimenter to modulate the parameters involved, like temperature, ionic atmosphere, concentration of the involved species based on the nature of the attractive potential. The essential component of a complex coacervate is a polyelectrolyte, such as poly-L-Lysine (pLL) in a very well-known poly-L-Lysine/Adenosine Triphosphate (pLL/ATP) system. In such systems, the coulomb interactions between the positively charged polypeptide and the negatively charged small molecule are exploited to fabricate condensates at around neutral pH typically performed at around pH ~ 7.4, i.e. physiological condition. These are known as complex coacervates and studies have been performed showing condensation not only in free solution but within vesicles, like liposomes, akin to organelle formation within cells. Complex coacervation of various kinds involving a wide variety of macromolecules have been studied by multiple groups all over the world using a diverse array of experimental tools.[6-18]

Experimental investigations of complex coacervation have been complemented by a series of theoretical studies[19,20] employing mean field theory,[21-23] Molecular Dynamics simulation,[24-28] Brownian Dynamics simulation[29-31] and Monte Carlo[32-37] simulation. In general, atomistic simulations have been avoided due to the inherent structural complexity of the polyelectrolytes involved and some amount of coarse graining has almost always been employed. Also, the general trend has been to replace the aqueous medium by its effect on the participating molecules. This is referred to as the implicit solvent model or the fluid particle dynamic model. These studies have tried to find the effects of salt concentration, polymer length or concentration and the distribution of charges on coacervation. Recently, there has been an attempt to find the driving force behind coacervation and identifying it as an entropic force.[25] However, more recently, a coarse-grained MD simulation has explored the dynamics of a transition between a polymer network forming phase to multiple coacervates as the polymer concentration is lowered, without assuming any such entropic forces.[28] Thus, the exact nature of the driving force remains debatable.

It is, however, more important to note, that in spite of such a rich legacy of studies, certain basic issues regarding complex coacervation remain unresolved. Of these, the foremost is the lack of any predictive theory for the critical value of the ratio of the participants for coacervation. Nor is there any clear idea about the structuration or charge distribution within the coacervate. In fact, it is only in the above MD study there is any direct demonstration of multiple coacervates being formed.[28] It is also to be noted that the dominant effect of the aqueous medium, namely, the hydrophobic repulsion felt by the participants which translates into an effective mutual attraction has never been modelled and has been represented by an empirical term.[28] This has, to our understanding, become a major impediment to an understanding of coacervation based simply on two body interactions or forces.

Moreover, we have found it surprising that there has never been any attempt to probe independently the validity of the coarse-grained models of the polyelectrolytes involved in LLPS. For example, pLL in water is uniquely characterized by the formation of fibrils at room temperature and high pH and of sheets at high temperature and high pH.[38,39] We strongly believe that understanding the pLL-pLL in aqueous medium is the essential requisite for any attempt to build a predictive model of pLL-ATP coacervation.

To provide some answers to the queries above, we have carried out an implicit solvent MC simulation study on the complex coacervation of pLL and ATP. We have used a very simple coarse grained models for both pLL and ATP, and have shown that a predictive model for the coacervation can be obtained entirely from two body interactions such as screened coulomb forces with an effective charge that mimics the pH and a screening parameter which we have reserved for counterions, Lennard Jones stabilizing potentials for both intra and inter molecular interactions, and, most important, an additional attractive square well potential with a Lennard Jones ‘tail’ and a range scaled by the simulation volume to model the ‘attraction’ between pLL molecules caused by the hydrophobic repulsion.[40] We hypothesize that our simulation based on a trade-off between coulombic and hydrophobic interactions, provides a simple yet effective way to a probable equilibrium structure consisting of pLL strands wrapping around the ATP molecules at room temperature, which has been validated by experiments.

We have initiated our study by reproducing the phase transitions of pLL in absence of ATP at high pH and at different temperatures. This study confirmed the importance of the hydrophobic interaction in the phase transition, validating our choice of the interaction potential. It also provided us with realistic estimates of the effective charge at high pH, and, more importantly, the value of the reduced temperature that corresponds to RT. This is dealt with in the first part of this communication.

With these estimates, we proceeded to simulate the LLPS process at lower concentrations. This simple model demonstrated quite accurately the formation of multiple coacervates, which not only tallied with those found for the afore mentioned much more time-consuming MD simulation at very large time scales, showing that the structures have by all probability reached the desired equilibrium and also closely resemble the coacervates experimentally observed. However, the most important achievements are, a) A reasonable estimate of the critical pLL/ATP ratio, and, b) The probable radial charge distribution inside the coacervates. This has been discussed in the second part of this paper. In this initial study reported here, we have not introduced any counterions or varied the temperature. These will be taken up in subsequent studies. We would like to add that our method is general enough to be extended to any complex coacervation.

2. Simulations on pLL in Aqueous Medium

2.1. The Model

As mentioned in the introduction, our model involves a degree of coarse graining. Hence, we have represented the positively charged pLL chains as sequences of 10 beads where each bead contains three monomers. We have chosen alpha pLL as our system, where the amine groups in the lysine groups remain positively charged at neutral pH or near neutral pH (~7.4) in water at RT, as illustrated in Figure 1. These conditions are of huge importance as at significantly alkaline conditions (pH around 11.0) the protonated amines get deprotonated, leading to charge neutralization. These charge neutralized polymers come close to one another due to hydrophobic interactions and form nanosized bundles/fibrillar structures at 25°C, which have been visualized using electron microscopy.[38,39]

The spherical beads have been connected sequentially by rigid bonds having a fixed length of 'σ', where σ denotes the bead size but the bonds are allowed rotations through 120° to maintain conformational flexibility as well as self-avoidance. A total of 100 such chains were placed randomly in a cubic simulation box of edge length '*L*' equal to 25σ, thereby yielding a number density of 'ρ'(N/L^3) having a value of around $6.4 \times 10^{-3}\ \sigma^{-3}$, to mimic a high concentration of the polymers in the aqueous medium. Periodic boundary conditions were imposed along the three dimensions and the minimum image convention was applied consistently for all pairwise interactions. The choice of ten-bead chains was motivated by the need to maintain the conformational flexibility of pLL sequences and arriving at a model that can be analysed with optimum tractability at any point once it reaches the desired equilibrium condition subjected to the relevant parameters and interactions. The simulation box size corresponded to a dense solution of the molecules.

For coacervate formation, very low pH (highly acidic) or very high pH (highly basic/alkaline) conditions are physically meaningless as ATP can tolerate a very narrow pH window of about 6.8 to 7.4. Beyond this, the molecule is not stable and ineffective.[13] However, in our paper we intend to prove or validate that our sequences are indeed pLL sequences by testing the structures at extreme pH values as the observed formation of fibrils happens at such high pH.[38,39] This compensates for the gross simplification of the structural complexity of the polymers as chains containing beads.

We also tested different temperatures by observing the equilibrated structures for different scenarios where we assign the value for which the outcomes look the most reasonable as room temperature, again comparing with the fibril formation at that temperature.

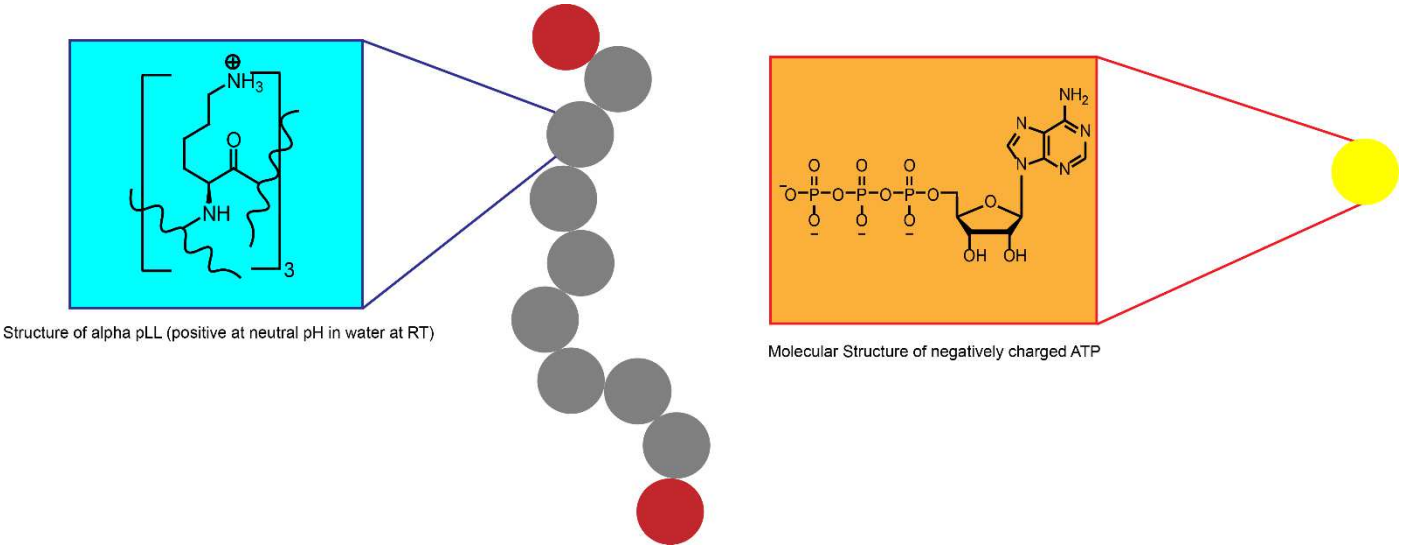


Figure 1. Schematic Representation of the (left) coarse-grained 10 beads alpha poly-L-Lysine (pLL) model and (right) single bead Adenosine Triphosphate (ATP) chosen for the MC simulation. Each bead corresponds to three monomers of L-Lysine having three positive charges at neutral pH and room temperature. The terminal beads are coloured differently for visual clarity. The ATP bead contains the relevant number of negative charges.

We have chosen the following potentials for our model system of pLL chains:

The screened Coulomb potential

$$(1)\ V_{sc}(r) = frac\, w_{11}\frac{e^{-\kappa r}}{r},\ r \le 0.3L,\ L = boxsize$$

where κ is the inverse Debye screening length representing the ionic ambience that was kept unchanged at $\kappa = 0.3\sigma^{-1}$, corresponding to a screening length of $3\sigma = 7$. The interaction strength is captured in the quantity *frac*, which is the effective charge of each chain and mimics pH of the medium, and the coupling factor w_{11}, whose magnitude has been normalised by the reduced temperature T^*, i.e. the effective coupling scales as w_{11}/T^*. This captures the effect of the aqueous medium on the charged moieties of the polymers. Increasing *frac* or decreasing T^* therefore amplifies electrostatic repulsion between chains, promoting chain extension and stiffening.

The Self-avoiding Lennard-Jones (LJ) potential[40]

$$(2)\ V_{LJ}(r) = \begin{cases} 4\left(\left(\frac{\sigma}{r}\right)^{12} - \left(\frac{\sigma}{r}\right)^{6}\right), & r \le r_{min} \\ 0, & r > r_{min} \end{cases}$$

where, $r_{min} = (2)^{\frac{1}{6}}\sigma$, and this stabilizing potential acts between all non-bonded bead-pairs and is very efficient due to its short range. The choice of $r_{\min}$ is consistent with the effective excluded volume of the side chains at the coarse-grained level, where σ is the unit of length and ε is the unit of energy.

The Hydrophobic interaction potential

$$(3)\ V_{hyd}(r) = \begin{cases} -\varepsilon_{att}, & r_{min} < r < r_{min} + w_F \\ 4\left(\left(\frac{\sigma}{r-w_F}\right)^{12} - \left(\frac{\sigma}{r-w_F}\right)^{6}\right), & r_{min} + w_F \le r \le w_F + r_{cut} \\ 0, & r > w_F + r_{cut} \end{cases}$$

This is modelled as a square-well-type potential from r_{min} to $r_{min} + w_F$, where $w_F = 0.25\sigma$ is the well width. Within this range the pair interaction energy equals $-\varepsilon_{att}$, the polymer-polymer attraction generated by the hydrophobic repulsion ε_{att}. This potential merges with a Lennard-Jones tail spreading to a global cutoff $r_{cut} = 2.5\sigma$, pairs with separation equal or greater than this cutoff experiencing no interaction.[40] This potential acts between all non-bonded bead pairs that do not belong to the same chain, consistent with the fact that polymers do not curl due to this repulsion but are only pushed together.

2.2. Details of the Monte Carlo Algorithm

All simulations were performed in the canonical (*NVT*) ensemble using the standard Metropolis Monte Carlo (MC) algorithm. Two complementary trial move types were implemented to ensure efficient sampling of both translational and conformational degrees of freedom.

The first move is a rigid-body translational displacement, in which an entire chain is selected at random and shifted by a random vector drawn uniformly from a cube of edge $2\Delta r_{max}$. After checking for hard-core overlaps with all other chains, the move is accepted or rejected according to the standard Metropolis criterion, $\exp(-\Delta U/k_BT)$. The second move involves internal conformational reorganisation via a sequential pivot algorithm starting from the second bead and proceeding along the backbone, each bead is relocated to a new position drawn uniformly on the sphere of radius b centred on its predecessor, subject to both the self-avoidance and bond-length constraints. A maximum of 40 attempts is made per bead before the previous position is retained if no valid new placement is found. This pivot-chain scheme efficiently samples the accessible conformational space of semi-flexible chains, particularly at low temperatures where direct displacement of individual beads would have poor acceptance.

The maximum displacement Δr_{max} was adjusted every 50 steps throughout each simulation to maintain a translational acceptance ratio of approximately 50%. The initial value was set to $\Delta r_{max} = 1.0\sigma$. All runs were initialised from a pre-equilibrated configuration, and the first 10% of steps in each production run were discarded to allow for additional equilibration. Structural observables were sampled every 1,000 MC steps over the remaining trajectory.

2.3. Key Structural Observables

At each sampling interval, the following chain-level structural quantities were computed and averaged over all 100 chains. The end-to-end distance $\langle R_{ee} \rangle$ is the Euclidean distance between the first and tenth bead of each chain, computed with the minimum image convention to handle chains that span the periodic boundary. The radius of gyration $\langle R_g \rangle$ is calculated from the mean-squared displacement of each bead from the chain's centre of mass. Together, the dimensionless ratio $\langle R_g \rangle / \langle R_{ee} \rangle$ provides a shape descriptor that is sensitive to chain architecture. A gaussian random coil yields $\langle R_g \rangle / \langle R_{ee} \rangle$ which is equal to $1/\sqrt{6} \approx 0.408$, while a perfectly rigid rod gives $1/\sqrt{12} \approx 0.289$.

Local chain stiffness was quantified through the inter-bead bond angles θ_k (k = 1, …, 8), defined as the angle between successive bond vectors along the backbone. A bond angle of 0° corresponds to fully extended (collinear) consecutive bonds, while non-zero angles reflect bending. The effective persistence length L_p was estimated from the integrated local curvature along each chain backbone, providing a single scalar measure of chain stiffness.

2.4. Results and Discussions

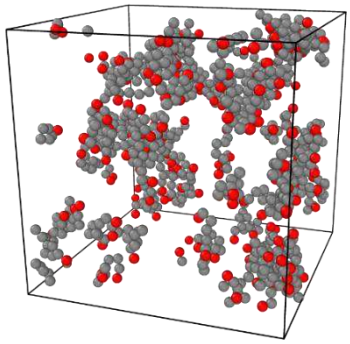
2.4.1. Effect of temperature

Table 1

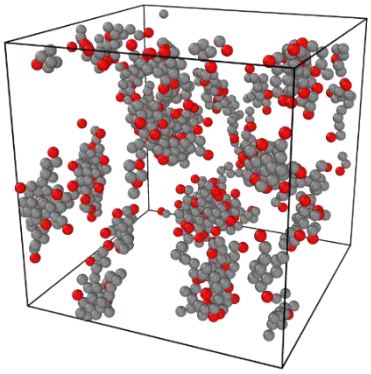
Reduced Temperature (T^*)	End Potential v_{End} (ε)	End to end distance $\langle R_{ee} \rangle$ (σ)	Radius of gyration $\langle R_g \rangle$ (σ)	$\langle R_g \rangle$ / $\langle R_{ee} \rangle$	Persistence Length L_p (σ)
0.5	+508.8	4.781	3.496	0.731	1.497
1.0	−1122.1	3.917	2.738	0.699	1.257
2.0	−2513.9	3.807	2.869	0.753	1.475
3.0	−1815.6	3.674	2.285	0.622	1.418

4.0	−1041.2	3.645	3.120	0.856	1.280
5.0	−764.5	3.597	2.949	0.820	1.308

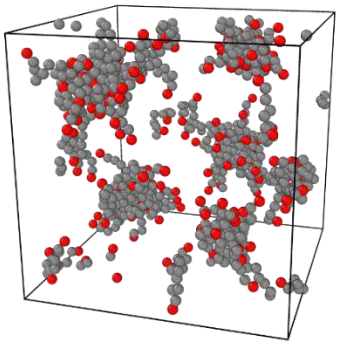
Table 1. Effect of Temperature. All runs use N = 100 chains containing 10 beads each, $L = 25\sigma$, $\sigma = 1.0$, $\kappa = 1/3\ \sigma^{-1}$, $r_{min} = (2)^{1/6}\sigma$. Effective charge per bead, *frac* = 0.05, Coulomb pre-factor, $w_{11} = 4.0$, Hydrophobic interaction potential well width, $w_F = 0.25\sigma$, Hydrophobic interaction potential well depth = 0.15.



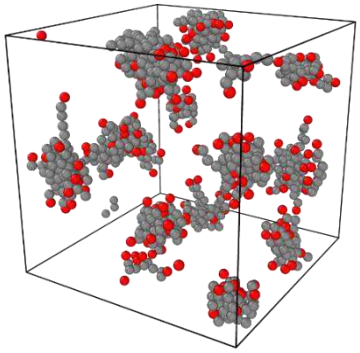
a



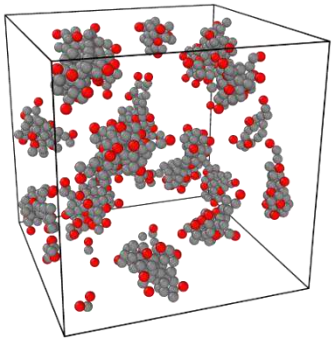
b



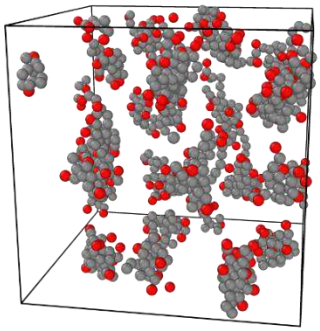
c



d



e



f

Figure 2. Simulation results of the 100-molecule model pLL system corresponding to different reduced temperatures (T^*) at monomer charge fraction (*frac*) = 0.05 and hydrophobically induced attraction (ε_{att}) = 0.15. a) T^*=5, b) T^*=4, c) T^*=3, d) T^*=2, e) T^*=1, and f) T^*=0.5. Refer text for details. pLL molecules are represented by grey beads with red beads at the termini (Figure 1).

Table 1 and the snapshots of the pLL as the results presented in Figure 2 show that, for a fixed monomer charge fraction and hydrophobic attraction, the macromolecules exhibit a strong dependence on the reduced temperature. As expected, the effect of temperature, or the corresponding thermal energy, is largely overcoming both the electrostatic repulsion and short-range forces like the Lennard-Jones repulsion and the hydrophobic attraction. The competition between these ordering forces and the disorder created by temperature is seen in Table 1 in the fluctuating values of the final potential energy and the structural parameters other than $<R_{ee}>$, which increases monotonically as the temperature decreases showing a straightening of the chains as the system is cooled and ordering forces start to dominate.

In the range T^* = 2–5, $<R_{ee}>$ remains in the narrow band 3.6σ –3.8σ despite a 2.5-fold change in temperature, and the total energies are all negative. This much weaker temperature sensitivity in this regime suggests that the attractive interactions more effectively counterbalance the electrostatic repulsion, leaving chain dimensions largely insensitive to modest thermal fluctuations.

The role of temperature can be most striking between T^* = 1.0 and T^* = 0.5. Reducing the temperature by a factor of two causes a substantial elongation of the chains: $<R_{ee}>$ increases from 3.92σ to 4.30σ (~10%), and $<R_g>$ rises from 2.74σ to 3.12σ (~14%). The persistence length increases, from 1.26σ to 1.37σ, indicating a clear stiffening of the backbone. The shift in the final potential energy from −1122ε to 428ε is particularly revealing as the system undergoes a crossover from a net-attractive to a net-repulsive regime. This happens due to the long-range electrostatic repulsion overcoming the short-range hydrophobic attraction. The formation of rigid chains at linear configurations, maximized at T^* = 0.5, shows excellent match with linear rigid fibrillar structures at 25°C.

A more comprehensive picture of the system evolving with temperature emerges from Figure 2, with the polymers moving away from each other and assuming disordered and randomised configurations as the temperature is increased. At higher reduced temperatures, especially at T^* = 5, we see a more or less uniform distribution of polymers indicating a high degree of disorder. This has a resemblance with the polymer networks observed at high concentrations and high values of the hydrophobic interaction in MD simulations.[28] At lower reduced temperatures this uniform distribution breaks down and clusters are formed. At T^* = 1 and finally 0.5, we clearly see the strands coming close to each other showing a tendency to assemble. However, the inter-bead repulsion because of the positively charged monomers prevents the formation of agglomerates and maintains a reasonable balance between attraction and repulsion, leading to well defined fibrillar bunches. We propose this to be the optimized condition where neither the repulsion nor the attraction dominates. This balance is imperative to use this pLL system as a functional macromolecular dispersion, such as formation of coacervates with oppositely charged molecules like ATP. Hence, we consider a reduced temperature of 0.5 to be the ambient temperature or room temperature for our model since the corresponding simulation shows the configuration closest to the fibrils observed in experiments. It may be noted that the uniform distribution at T^* = 5 bears some resemblance to the pLL sheets observed at high temperatures (40.6°C).[38,39]

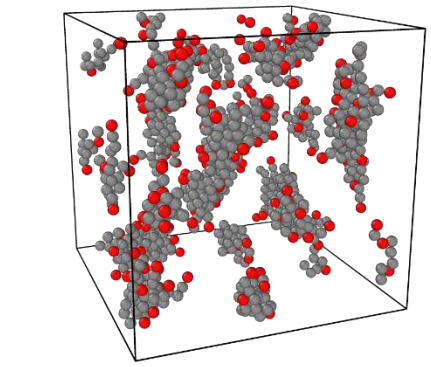
Effect of the Bead Charge and Hydrophobic Interaction on the Polymers

Table 2

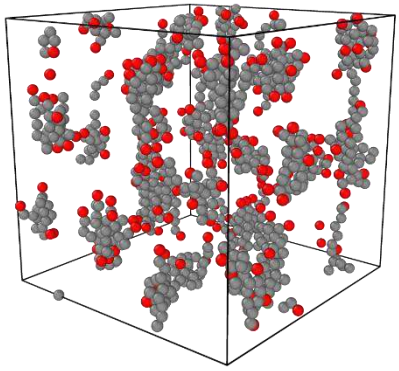
Effective Charge per bead (*frac*)	Hydrophobic Attraction (ε_{att})	End Potential v_{End} (ε)	End to end distance $<R_{ee}>$ (σ)	Radius of gyration $<R_g>$ (σ)	$<R_g>$ / $<R_{ee}>$	Persistence Length L_p (σ)
0.05	0.15	+427.5	4.297	3.119	0.726	1.367
0.06	0.15	+918.2	5.137	3.677	0.716	1.605

0.07	0.15	+1374.6	5.337	3.571	0.669	1.795
0.08	0.15	+1851.6	6.025	3.804	0.631	1.609
0.08	0.00	+1912.1	6.457	4.308	0.667	1.879

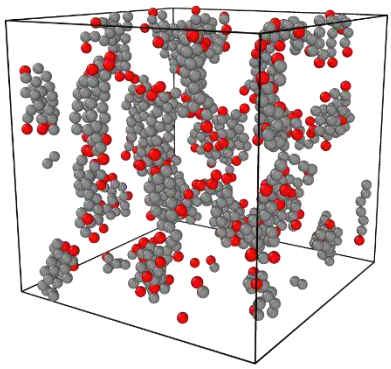
Table 2. Effect of Bead Charge and Hydrophobic Interaction. All runs use N = 100 chains containing 10 beads each, $L = 25\sigma$, $\sigma = 1.0$, $\kappa = 1/3\ \sigma^{-1}$, $r_{min} = (2)^{1/6}\sigma$. Reduced temperature, $T^* = 0.05$, Coulomb pre-factor, $w_{11} = 4.0$, Hydrophobic interaction potential well width, $w_F = 0.25\sigma$.



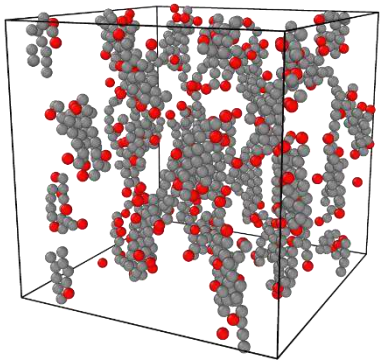
a



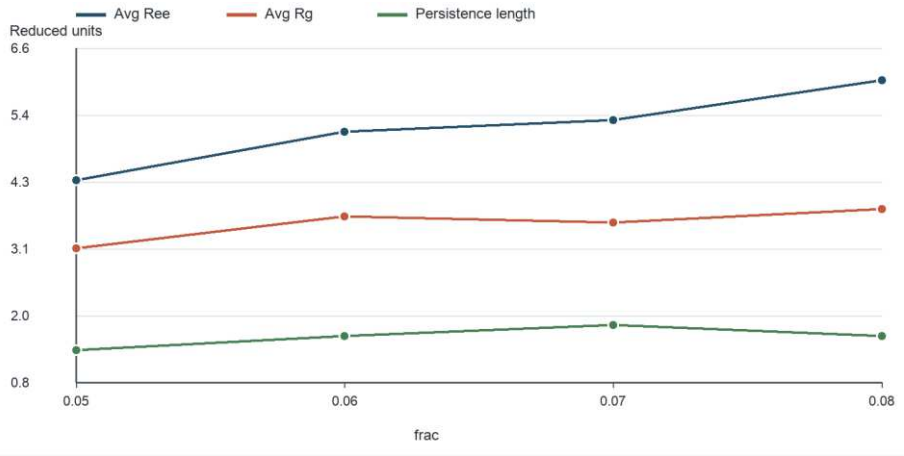
b



c



d



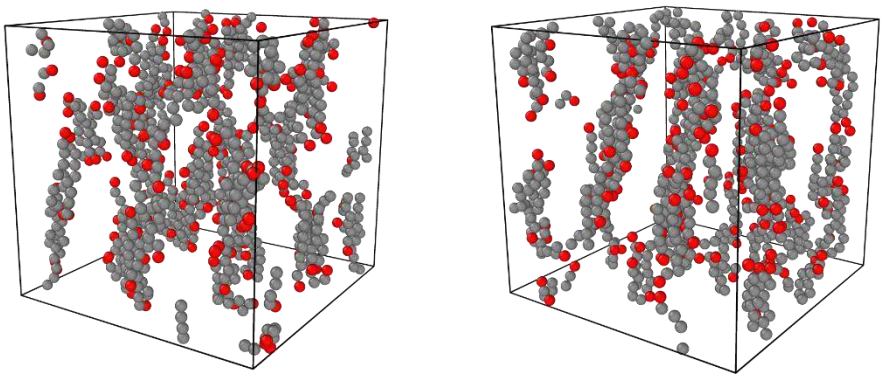
e

Figure 3. Simulation results of the 100-molecule model pLL system corresponding to different monomer charges (*frac*) at fixed T^*= 0.5 and hydrophobically induced attraction (ε_{att}) = 0.15. a) *frac* = 0.05, b) *frac* = 0.06, c) *frac* = 0.07, d) *frac* = 0.08. e) Variation of average end to end length (<R_{ee}>), average radius of gyration (<R_g>) and persistence length (L_p), all in reduced units, with *frac*.

While the roles of the effective charge on the beads of our model, i.e. the Coulomb repulsion and the attraction caused by hydrophobic interaction are shown quantitatively in Table 2, Figure 3 and Figure 4 show, through sequences of snapshots from simulation runs, respectively, the effect of the charges and of the hydrophobic interaction on the model system. As mentioned earlier, each bead in the simulation represents three monomer units. In other words, each bead is tripositive at near neutral pH or physiological pH. When subjected to extremely alkaline or very high pH conditions, the positive charges coming from the protonated amines in the lysine monomer units get deprotonated. This prompts the polymers to come close to each other and form fibrillar structures, which have been experimentally observed at a pH > 10 using electron microscopy. In our simulation we have replicated the variation of charge distributions due to an effect akin to deprotonation by modulating the parameter *frac*. We now look at the quantitative analysis corroborating these observations in Table 2.

Even within the narrow window of the effective charge fraction *frac* 0.05 to 0.08 at fixed T^* = 0.5 and hydrophobic attraction ε_{att} = 0.15, the structural response is significant. As *frac* increases from 0.05 to 0.08, <R_{ee}> rises monotonically from 4.30σ to 6.02σ — a 40% increase — while <R_g> grows from 3.12σ to 3.80σ an increase of 22%. The persistence length increases from 1.37σ to 1.61σ though *frac* = 0.07 gives the highest single value of 1.80σ, likely reflecting its considerably longer sampling time of 500,000 steps which reduces statistical fluctuations. All these confirm backbone straightening with larger effective charge. The end-potential energy rises steeply with *frac*, rising from 428ε to1852ε. As the number of electrostatically interacting pairs grows roughly as the square of the number of charged beads, and each bead carries a screened coulomb repulsion whose magnitude is proportional to the product of *frac* and w_{11}/T^*, a small increment in the charged fraction has a disproportionately large effect on the total energy. This non-linear amplification is expressed in the steep <R_{ee}> versus *frac* response observed here.

Again, the effect of this charge increase is exhibited more dramatically in the formation of bunches of vertically aligned chains, consistent with the experimentally observed pLL fibrils at high pH and room temperature. As is evident from the snapshots, and more quantitatively from Figure 3(e), there is no marked variation in the pLL dispersion when we go from 0.05 to 0.08 in the value of this charge parameter. However, we choose 0.08 to be the most reasonable charge value as it corresponds to the configuration with the greatest end to end distances.



a **b**

Figure 4. Simulation results of the 100-molecule model pLL system with and without hydrophobic attraction (ε_{att}) at fixed T^*= 0.5 and *frac* = 0.08. a) ε_{att} = 0.15, b) ε_{att} = 0.0.

Figure 4, and the last two rows of Table 2, clearly show the difference between the presence and absence of the hydrophobic interactions. In presence of the hydrophobic attraction for the optimized reduced temperature and monomer charge fraction, namely T^* = 0.5 and *frac* = 0.08, we see the desired balance between attraction and screened coulomb repulsions leading to the configuration which the pLL dispersion most likely assumes at RT at high pH (>10). In the absence of the attractive potential, we see a uniform distribution all over the three-dimensional space and no tendency to form the fibres observed at the same temperature and pH.[38,39] Hence, we can arrive at the conclusion that the compromise between coulombic repulsions and hydrophobic attractions is what leads to the pLL configurations which give rise to the phases that we are familiar with based on experimental studies. In particular, it underscores the importance of the hydrophobic interaction. Let us again look at the quantitative information in Table 2.

Comparison of ε_{att} = 0.15 with ε_{att} = 0.00 at otherwise identical conditions of T^* = 0.5, *frac* = 0.08, w_{11} = 4.0, i.e. the last two rows of Table 2, brings out the contribution of the hydrophobic flat-well interaction. Removing the attractive well increases $\langle R_{ee} \rangle$ from 6.02σ to 6.46σ (~7% increase) and $\langle R_g \rangle$ from 3.80σ to 4.31σ (~13% increase), while the persistence length rises from 1.61σ to 1.88σ, confirming that the hydrophobic interaction introduces a modest but measurable attractive force that partially counteracts the electrostatic extension.

The total energy increases from 1852ε to 1912ε, a relatively small increase of ~ 60ε. This tells us that, at these conditions, the hydrophobic interactions contribute only a small fraction of the total interaction where the dominant term is the long-range screened coulomb repulsion. In contrast, the structural effect on chain dimensions is non-trivial and clearly discernible above statistical noise, which underscores the sensitivity of chain conformation to even weak inter-chain attractions at low temperature. From a biological standpoint, this balance is meaningful: the hydrophobic patches on pLL side chains provide a handle for mediating compaction or aggregation that would otherwise be suppressed by the strong coulombic repulsion at near neutral pH.

Parameters dictating the Conformation of the Macromolecules

The effective persistence length L_p ranges from approximately 1.26σ to 1.88σ across all runs reported here. The contour length of the ten-bead chain is L_c = 9σ, so L_p/L_c is in the 0.14–0.21 range. Thus, the chains are in the flexible-to-semiflexible crossover regime. Under the worm-like chain (WLC) model, a chain with $L_p/L_c \approx 0.20$ would exhibit $\langle R_{ee}^2 \rangle \approx 2L_pL_c \approx 3.6\sigma^2$, or $\langle R_{ee} \rangle \approx 1.9\sigma$. Our observed $\langle R_{ee} \rangle$ values are considerably larger, varying from 4σ –6σ. This additional length is due to inter-chain excluded volume and, more importantly, the strong screened coulomb repulsion that stretches the chains beyond that predicted by the neutral WLC model. Our model pLL chains are thus better described as partially swollen coils that are largely rigid due to the coulombic repulsions and not as worm like chains.

The ratio $<R_g>/<R_{ee}>$, which decides the shape, has higher values in the high-temperature, attractive regime. Here chain dimensions are relatively compact and the gyration radius becomes comparable to the end-to-end distance, which indicates some degree of non-linearity such as ring-like or folded configurations. At $T^* = 0.5$, the ratio stabilises at around 0.63–0.73, a range that reflects elongated but significantly fluctuating conformations. Combined with the high persistence lengths, this suggests a population of relatively straight, rigid configurations.

Crossover from Hydrophobic Attraction to Screened Coulomb Repulsion

One of the more striking features emerging from the data is the change in sign of the final potential energy v_{End} as the system shifts from high to low temperatures. In the former regime, v_{End} is highly attractive, reflecting a system in which attractive interactions, either the hydrophobic flat well or, more likely, effective pair attractions mediated by the combined potential, dominate the total energy. In contrast, all $T^* = 0.5$ runs yield positive v_{End} values. This transition marks a fundamental change in the free energy landscape: at low temperature and with a sufficiently large charged fraction, the screened coulomb repulsion between chains completely dominates, suppressing any tendency for inter-chain contacts and driving the system into a dilute, chain-extended state. The energy conservation was verified for all runs, confirming numerical stability of the integrator across this range of conditions.

Comparison with Observed pLL Structures

The results of the NVT Monte Carlo simulation reported here reveal a number of trends in the structural changes of pLL polyelectrolytes subjected to a 'guess potential' . The effective length and rigidity of the chains increase with the charged monomer fraction and decrease with temperature, behaviours attributable to the temperature-renormalised screened coulomb repulsion that features with weight w_{11}/T^*.

Hydrophobic attraction for the magnitude $\varepsilon_{att} = 0.15$ contributes a secondary compaction effect that partially counteracts electrostatic extension without reversing it. The sign reversal of the total potential energy between the higher- and lower-temperature runs signals a qualitative change in the dominant energetic balance of the system.

Our findings perfectly tally with experimental results obtained at high pH and ambient temperature, where the charges on the polyelectrolytes (positive) get neutralized as they get deprotonated at pH ~ 11.8 and 25°C leading to the formation of pLL fibres.[38,39] In our model, we see similar aggregate formation or 'bunching' for low values of charges on the monomers, corresponding to the value of *frac* ranging from 0.05 to 0.08 and $T^* = 0.5$. This enables us to set this value of the reduced temperature equal to the physical temperature of 25°C and the charge fraction within 0.05 and 0.08 corresponding to pH ~ 11.8. We also find that the bunching of the pLL macromolecules is significantly enhanced in presence of the hydrophobic interactions, which is the most significant observation of this simulation study. To the best of our knowledge, this work is the first attempt towards delineating the interplay of short-range attractions and long-range repulsions quantitatively, which gets rid of a rough qualitative description. There is no empiricism involved in our simulation, where different regimes have been thoroughly tested by systematically varying the charge, temperature and by taking into account the pre-exponential factor for a given screening length. Thus, through the consistence with the observed behaviour of pLL we have established our model of pLL and the relevant interactions deciding its structural phases. This shall enable us to proceed to the next step, i.e., simulating the pLL/ATP complex coacervation.

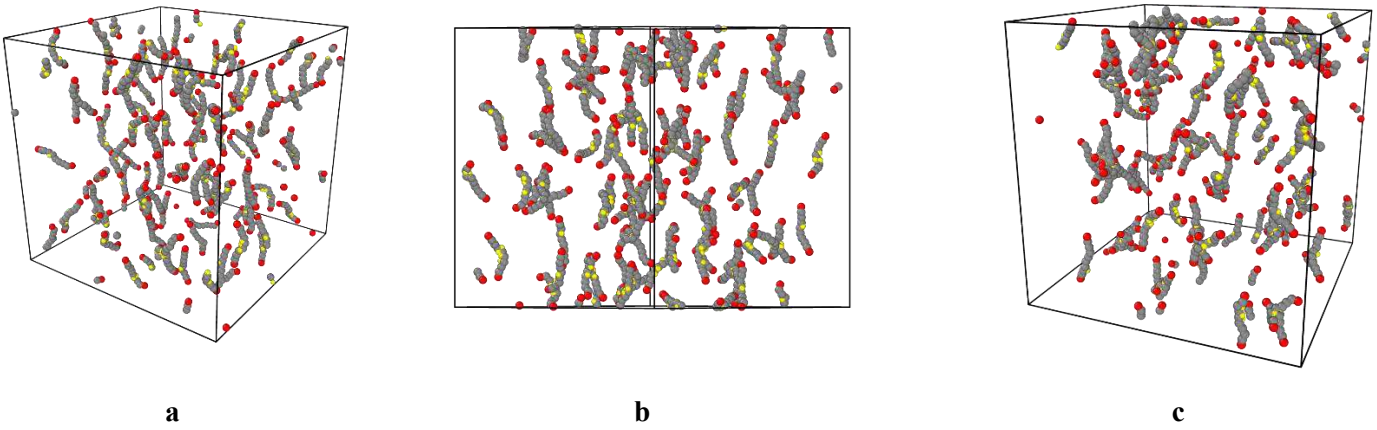
Simulation of pLL-ATP Complex Coacervation

Introduction of ATP and System Visualizations

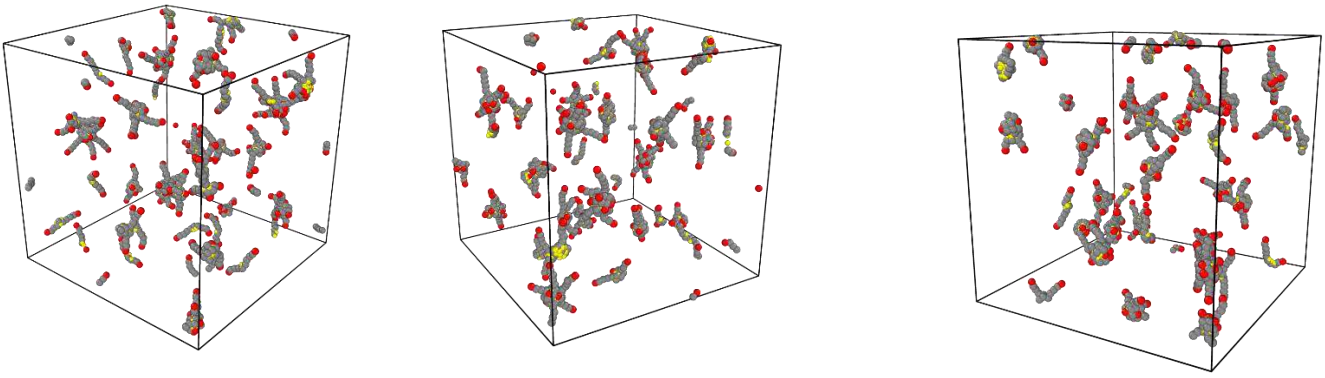
In the previous sections, we have established the chosen simple positively charged bead model to be a viable representation of a pLL chain. We now proceed with this model to perform pLL-ATP complex coacervation *in silico* keeping the temperature at RT ($T^* = 0.5$), and the values of the van der Waal and hydrophobic interactions unchanged for pLL. To conduct the LLPS simulation, we introduced negatively charged single beads which represent ATP molecules, as shown in Figure 1, interacting with the pLL beads through the attractive Coulomb force given by Eqn (1) with a negative sign. As LLPS takes place at neutral pH (~7.0) at RT [ref], where the ATP remains undamaged and both pLL and ATP are fully charged, we have chosen a *frac* value of 1.0, more than an order of magnitude above the value

chosen earlier for high pH. We assume this enhancement in Coulomb interaction to be a fair emulation of the pH ambience.

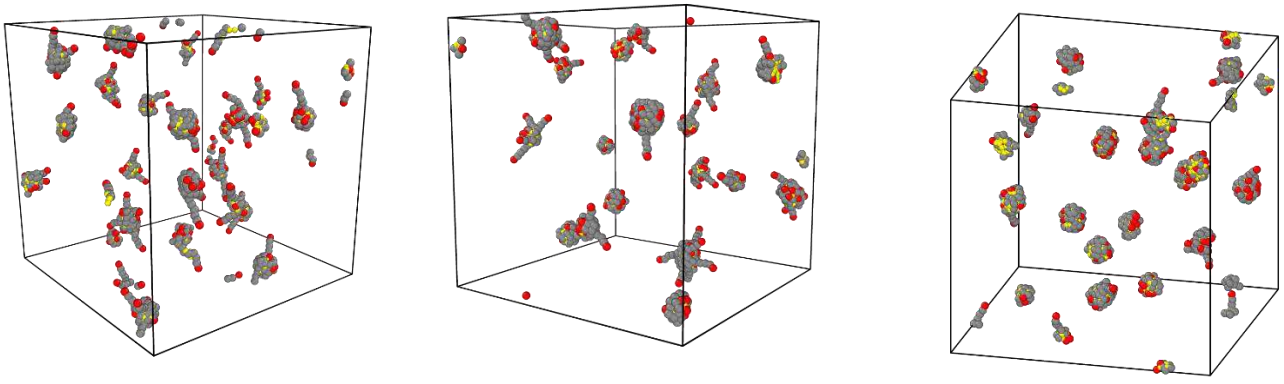
In this study we are focused on the precise value of the number of ATP molecules/pLL molecule, i.e. the ATP/pLL number ratio that is critical for initiation of complex coacervation, which to the best of our knowledge has not been determined or predicted in literature. To this end we have carried out simulations on systems with a considerable range of ATP/pLL number ratios, namely 2, 3, 4, 5, 6, 7, 8, 9, 10, and 15. In each case, 2 million simulation steps were performed to reach equilibrium. To keep the model simple, we have not considered ATP-ATP Coulomb repulsion and hydrophobically induced attraction between ATP molecules. We used a simulation box size of side 50σ each to simulate a dilute solution of the molecules.



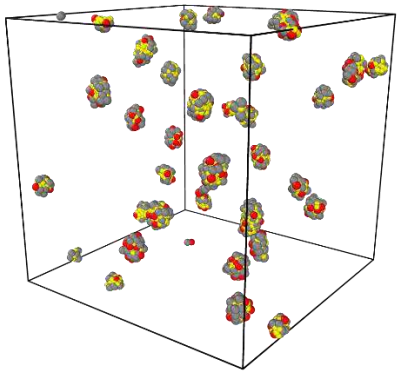
a **b** **c**



d **e** **f**



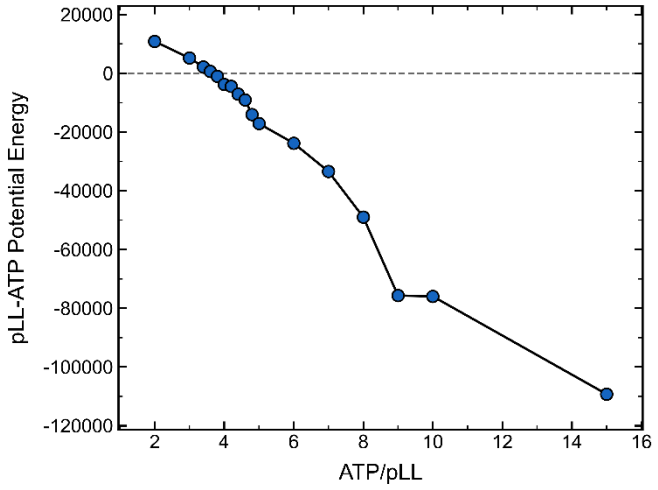
g **h** **i**



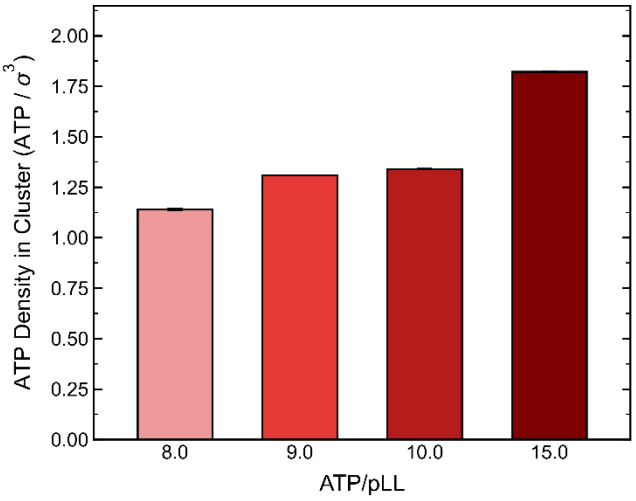
j

Figure 5. Simulation results from 2 million runs of the 100-molecule model pLL system corresponding to different numbers of ATP molecules/pLL molecule (ATP/pLL number ratios) at fixed T^*= 0.5 and effective charge *frac* = 1.0, a) 2, b) 3, c) 4, d) 5, e) 6, f) 7, g) 8, h) 9, i) 10, and j) 15. The ATP molecules are represented by single yellow beads while the pLL molecules are represented by grey beads with red beads at the termini (Figure 1).

Figure 5 shows representative snapshots of the systems at the end of 2 million simulation steps. As is evident from the figure, there is no nucleation for ATP/pLL values of 2, 3 and 4. Therefore, we can conclude that at relatively low ATP concentrations the transition from a repulsive regime to an attractive regime has not occurred. For a value of ATP/pLL equal to 5, we see the initiation of the LLPS process. This is clear from the formation of 'nuclei' where the strands and ATP molecules start to wrap around each other. However, these structures cannot be referred to as coacervates/condensates as fractions of the pLL threads are pointing outwards indicating a lack of complete energy minimization stopping the system from assuming a spherical shape. Thereafter, a gradual increase in the number of ATP molecules leads to the desired phase separated configurations. The first spherical structures typical of coacervates appear at ATP/pLL = 8, reaching the ideal scenario for values of 9 as well as 10, as is evident from the corresponding snapshots. The occurrence of LLPS, in particular the appearance of complex coacervates with this simple model is a major confirmation of its strength and indicates the dominant role of screened Coulomb interactions in deciding the critical ATP/ pLL ratio. It is to be noted that the structures from 8 to 10 are very similar to structures emerging at long times, low polymer concentrations, and comparatively high hydrophobic interaction values, in MD simulations[28] in agreement to the equilibrated character of these structures and the other parameters of our model.



a



b

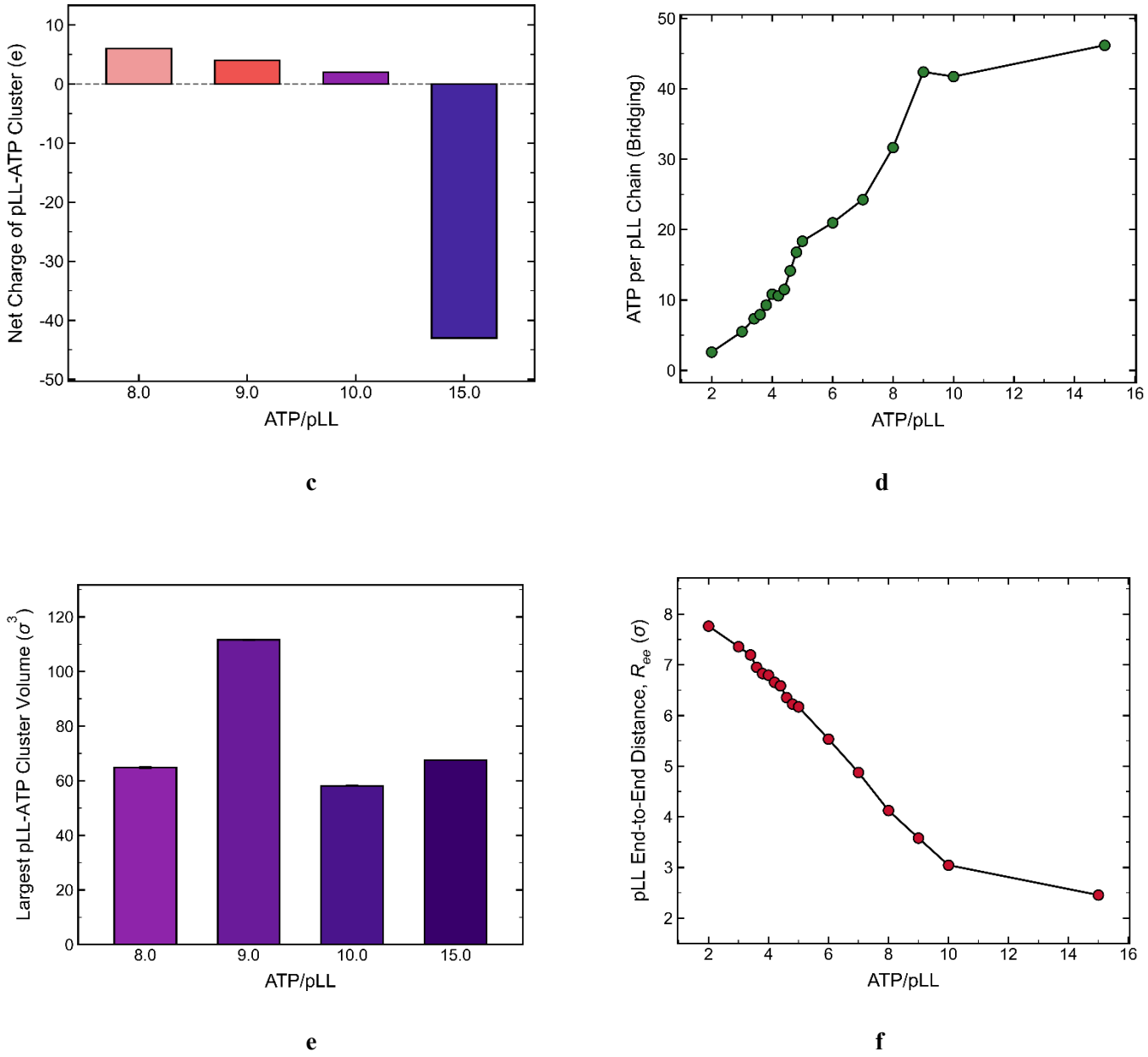


Figure 6. Physical parameters obtained from the systems represented in Figure 5. All parameters are obtained against variations in ATP/pLL ratio. (a) Total interaction energy in the system; (b) Average ATP density in each coacervate in ATP number σ^{-3}; (c) Average net charge of each coacervate; (d) ATP induced bridging quantified by average ATP number per pLL chain; (e) Maximum coacervate volume in σ^3; (f) pLL end-to-end distance R_{ee} in σ.

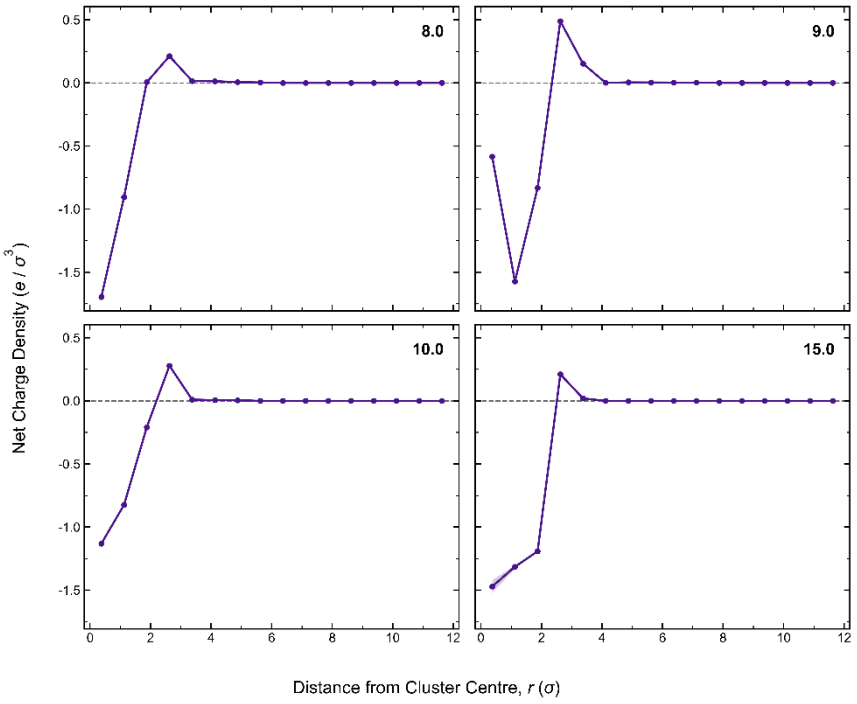
Figure 6 shows some important physical parameters obtained from the simulations. From Figure 6(a) revealing the variation of the overall interaction potential, we can clearly see the crossover from a repulsive regime to an attractive one upon sequential addition of ATP beads. This sheds light on the minimum number of ATP molecules required to see a phase change. Consistent with Figures 5(h) and 5(i), this graph reaches a plateau at ATP/pLL reaching 9 and 10 indicating charge neutralisation.

It is also interesting to note from Figure 6(b) that even beyond the charge neutralisation point, the clusters can accommodate an excess of ATP. This is highly instrtuctive as it shows that energy minimzation is not necessarily equal to charge cancellation in the case of superstructures such as the condensates in question. This is corroborated in Figure 6(c) which shows the variation of the net charge upon addition of ATP molecules. The change in direction of the last bar in the plot to negative values validate the fact that there is a large excess of ATP in the condesate system beyond the charge neutralization point. It is also seen that at values of 9 and 10 exact neutralisation is not achieved and there is a very small excess of positive charge. This excess of positive charge is consistent with the experimentally observed positive Zeta potential of pLL-ATP coacervates [ref] while the large excess negative charge is inconsistent. Thus, though

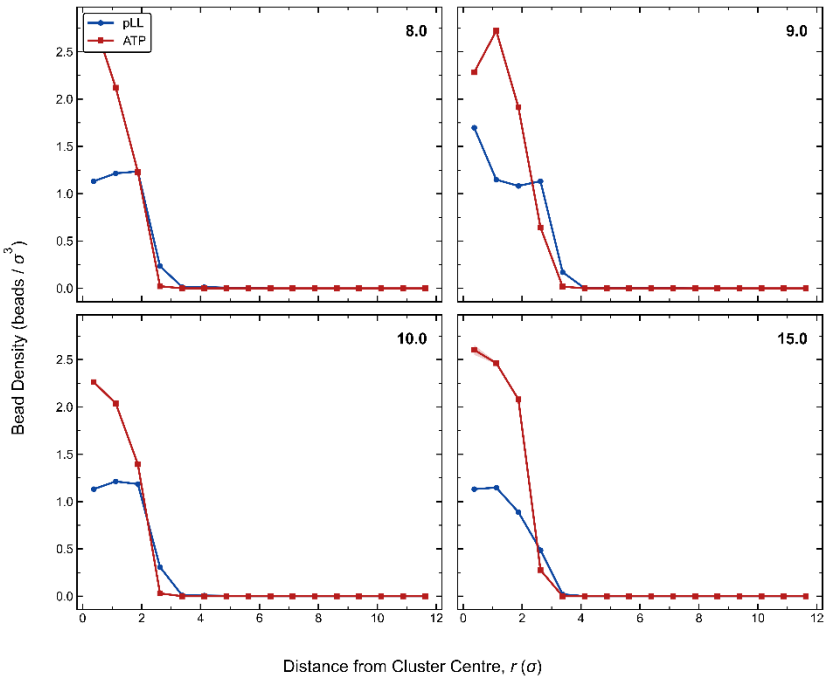
coacervates with calculable physical parameters are obtained beyond the ATP/pLL value of 10 in our simulation, addition of ATP beyond this value does not appear to be physically meaningful.

The close equivalence of the coacervations at 9 and 10 ratios is also reflected in Figure 6(d), where the average number of ATP molecules attached to a pLL chain shows a sharp rise from 8 to 9 and then in fact drops a little for 10. This plot is also significant because it shows close resemblance to the observed variation of turbidity with ATP concentration by the Dekker group[18], and there is a close correspondence between turbidity of the medium and the average number of ATP molecules attached to a pLL chain in a coacervate. The system at 9 apparently shows a special behaviour in Figure 6(e) in having the maximum average coacervate volume, which cannot be explained by strands of pLL pointing out since such strands are more for the 8 ratio. From 9 to 10 there is a significant cotraction in coacervate volume.

The variation of $<R_{ee}>$ as a function of pLL/ATP ratio (Figure 6(f)), quantifying the process of formation of spherical coacervates, shows an initial slow decrease below the ATP/pLL value of 5, after which it decreases with a steeper slope till reaching the value of 10. This is expected as neutralization is the key interaction leading to coacervation. Beyond this point the slope is not as sharp since the reduction in polymer length will be slower after all the positive charges have been quenched by ATP addition. In any case, as discussed above, going beyond 10 is not very meaningful.



a



b

Figure 7. Radial distributions of the key parameters dictating the coacervate structure. (a) Variation of net charge as a function of the radial distance (starting from the cluster centre). (b) Distribution of bead densities of pLL and ATP as a function of radial distances.

Figure 7 reveals the internal structure of the coacervates obtained from our study. This has not been clearly delineated till date to the best of our knowledge. In Figure 7(a), we see a gradual decrease in the negative charge density followed by a spike in the positive charge domain which subsequently falls and stabilizes at zero. From this distribution, it is evident that the core of the cluster is ATP dominated. As we move towards the surface of the cluster, the density of pLL beads increases leading to a steady cancellation of charges followed by a sudden increase in the pLL chain density (the spike in the plot) and a subsequent neutralization. The spike in the plot is the highlight of our analysis, as it perfectly matches with real pLL ATP condensates which have been measured to have a zeta potential (or surface potential) of pLL/ATP systems of around +14 mV to +18 mV (or neutral) for standard ratios. This charge density distribution is exactly corroborated by Figure 7(b), where the radial density distributions of ATP and pLL within the average coacervate, as obtained from our simulation, are shown. Again, the most interesting situation occurs at ATP/pLL reaching the value of 9. In contrast to a sharp fall in ATP and the negative charge from the centre to the periphery observed at the other ratios, there is a peak at around 1σ from the centre, somewhere around the middle of the coacervate. Simultaneously, instead of a small plateau followed by a gradual fall in pLL, as at the other ratios, there is a dip at about the same location. This suggests the formation of denser layer of ATP 'trapped' in a reduced layer of pLL, a fascinating probability to be explored experimentally.

In this communication of the results of Monte Carlo simulation studies our primary focus was to indicate the role of different intermolecular forces in determining the phase behaviour of poly-L-Lysine at high pH and liquid-liquid phase separation leading to complex coacervation in its interaction with Adenosine Triphosphate at near neutral pH, both at room temperature. We could achieve the essential features of both these experimentally observed phenomena using simple models of pLL and ATP, and thereby bring out the importance of Coulomb forces between pLL molecules and between pLL and ATP molecules, as well as the attraction between pLL molecules caused by hydrophobic repulsion from the aqueous medium.

We started by establishing our simple model of positively charged 10-bead strands to represent some major features of pLL by subjecting them to high pH like conditions, where the charges on the polymers get neutralized. This can also be achieved by introducing a counterion, but the physics behind pH rise, i.e. introduction of an alkali and adding negatively charged ions is not the same. In the former case it is a global, statistical effect as the hydroxyl ions abstract protons rendering the system chargeless. On the other hand, for a counterion like a halide ion from a salt will not abstract protons but simply stick to the positive ends cancelling the net charge. We propose that pH conditions can be simulated by tuning

the effective charge fraction (*frac*) of the pLL and ATP beads, whereas the effect of counterions can be dealt with by changing the screening parameter (κ). In this communication we have utilised the former, keeping its value low (0.08) for high and high (1.0) for near neutral pH. We would utilise the screening parameter for future studies. The formation of fibrils, consistent with observed results[38,391], established the values of the effective charge, of the effective room temperature, and of the van der Waals and the hydrophobic interactions. These were used in simulating the process of coacervation.

In the second half, we have succeeded in generating condensates by modulating the pLL/ATP ratio. This allowed us to predict the critical phase separation concentration ratio which is impossible to pin down using free energy arguments alone. An important added bonus of this is the unravelling of the internal structure of the coacervate which has remained a black box as of now, and which shows an intriguing structuration at the pLL-ATP ratio of 1:9. Since we are using a well-defined potential to give rise to the desired phenomenon, we can correlate the parameters in the potential function, like *frac* to the formed clusters. Thus, our results can be smoothly extended to other *frac* values, larger number of molecules and more complex molecular models, as well as introduction of ATP-ATP Coulomb repulsions and hydrophobic forces on ATP molecules. However, it is to be noted that the critical concentration ratio is also dependent on the value of this effective charge.

As has been discussed thoroughly in the introductory section, our study is based on a first principles implicit solvent model where water molecules are not physically present. This obviously affects the volume of the coacervates obtained from our simulations since water is a major component of coacervates. However, our interest has throughout been the unravelling of the forces behind coacervation and never the composition of actual coacervates.

Another highlight of our paper is the fact that the number densities and the critical point could be predicted from a simple Monte Carlo approach where the intricate structural details and molecular composition have not been considered. This validates the fact that this is not restricted to pLL or ATP alone but is true for any polymer/small molecule interaction where charges play the dominant role.

In spite of the fact that a relatively simple, coarse-grained model led to the formation of multiple complex coacervates making it largely a model which includes a number of such charged macromolecule/small molecule couples, it lacks certain structural details like the molecular details of the charged monomer units which have been encapsulated in the form of a charged sphere or bead. Moreover, we have not taken into account the possible hydrophobic interactions stemming from the pi moieties in the ATP molecules which can lead to both intermolecular attractions and strengthening of the adhesion to the macromolecules in question.

Another vital aspect which has not been investigated in the communication is the optimization of the pLL chain lengths. We cannot definitively state that the chosen polymer length is ideal or the critical chain size necessary to initiate the LLPS process discussed in the paper.

Conclusions and Outlook

In this communication, we have been able to show how the conformation of poly-L-Lysine (pLL) macromolecules depends on the interplay between screened coulombic repulsions and hydrophobic interactions using a Monte Carlo approach, which, to the best of our knowledge, is an uncharted territory. As a model of the polymer, we have employed a flexible strand of 10 beads, each representing 3 lysine monomers. We have accounted for the aqueous medium by using the included solvent approach. Here the effect of the medium is taken care of by the screening of the coulomb repulsion between the monomer charges and the attraction between the molecules caused by the hydrophobic repulsion from the medium. The effect of pH of the medium is simulated by the monomer charge fraction. As at high pH the monomers become deprotonated this fraction should have small values. We have tested the system at high pH and at different temperatures parametrized by a reduced temperature.

Our results clearly reveal that, at a high reduced temperature the strands are distributed almost uniformly over the simulation volume even at high pH, i.e., low monomer charge fractions. This has a faint resemblance with pLL sheets formed at pH > 10 and at temperatures of around 40°C. As the temperature is reduced a tendency to form bundles becomes visible. This shows that the thermal interaction is high enough to overcome the attraction between the strands, which is not surprising but is important to establish the model. Finally, the model showed the formation of bundles of rigid and vertically elongated strands closely resembling pLL fibrils that are observed to form at pH > 10 and at RT simultaneously the total intermolecular interaction changes from an attractive to a repulsive regime, which pushes the

strands to their rigid and elongated conformation. The corresponding reduced temperature is thus identified with RT. As for the monomer charge fraction it is observed that on changing the value from 0.05 to 0.08 there is no significant change in the configurations in these bundles, hence this entire range is consistent with the observed high pH conditions. However, the most important observation is that, on switching off the intermolecular short-range attraction caused by the hydrophobic repulsion from the medium, there is no bundle formation under these conditions. This indicates the importance of the hydrophobic interaction in determining pLL structuration. Thus, our simple model reproduces the main features of the structural transitions observed experimentally for pLL, without recourse to any consideration of specific molecular conformations, showing the defining roles of the intermolecular forces in these transitions. These results form the basis for investigations into liquid-liquid phase separation involving pLL and building a predictive model for coacervation.

In the second part of our paper, we could achieve coacervation at neutral pH and at RT. We have taken a radically new approach where we have correlated the changes in the charge distributions and potentials to the phase separation upon addition of ATP. We could arrive at the desired coacervates by sequential addition of ATP and could unravel the crossover point from an overall repulsive to an attractive regime. In addition to this, we could also find the radial charge and molecular distributions as well as the net charges of the formed clusters. This, to the best of our knowledge, is the first predictive model to unravel condensate formation and their internal structures, where a single thermodynamic parameter has not been invoked.

We plan to extend our studies to explore the effects of the effective charge, of the other interactions, of the temperature, and of added counterions in future communications. We strongly believe that this shall break new ground in the fascinating domain of the chemistry and physics of LLPS, as it is the first step towards constructing a phase diagram based not on the result but the forces dictating structuration.

Data Declaration

All data generated or analyzed during this study are included in this published article and its supplementary information files.

Funding Declaration

No funding.

References

1. Zhengyu Xu, Wei Wang, Yi Cao, Bin Xue, Liquid-liquid phase separation: Fundamental physical principles, biological implications, and applications in supramolecular materials engineering, Supramolecular Materials 2, 2023, 100049.
2. N. Amy Yewdall, Alain A.M. André, Tiemei Lu, and Evan Spruijt, Coacervates as models of membraneless organelles, Current Opinion in Colloid & Interface Science 52, 2021, 101416.
3. Alicja Napiórkowska and Marcin Kurek, Coacervation as a Novel Method of Microencapsulation of Essential Oils—A Review, Molecules 27, 2022, 5142.
4. Basusree Ghosh, Rudrarup Bose, and T.-Y. Dora Tang, Can coacervation unify disparate hypotheses in the origin of cellular life? Current Opinion in Colloid & Interface Science 52, 2021, 101415.
5. Dikesh Kumar Thakur, Sonal Padole, Tapati Sarkar, Somasundaram Arumugam, Shiladitya Chattopadhyay, Liquid–Liquid Phase Separation: Mechanisms, Roles, and Implications in Cellular Function and Disease, FASEB Bioadvances 7, 2025, e70054.
6. Damian Wollny, Benjamin Vernot, Jie Wang, Maria Hondele, Aram Safrastyan, Franziska Aron, Julia Micheel, Zhisong He, Anthony Hyman, Karsten Weis, J. Gray Camp, T.-Y. Dora Tang, and Barbara Treutlein, Characterization of RNA content in individual phase-separated coacervate microdroplets, Nature Communications 13, 2022, 2626.
7. Evan Spruijt, Frans A. M. Leermakers, Remco Fokkink, Ralf Schweins, Ad A. van Well, Martien A. Cohen Stuart, and Jasper van der Gucht, Structure and Dynamics of Polyelectrolyte Complex Coacervates Studied by Scattering of Neutrons, X-rays, and Light, Macromolecules 46, 2013, 4596.

8. Celina Love, Jan Steinkühler, David T. Gonzales, Naresh Yandrapalli, Tom Robinson, Rumiana Dimova, and T.-Y. Dora Tang, Reversible pH-Responsive Coacervate Formation in Lipid Vesicles Activates Dormant Enzymatic Reactions, Angew. Chem. Int. Ed. 59, 2020, 5950.
9. Karina K. Nakashima, Jochem F. Baaij, and Evan Spruijt, Reversible generation of coacervate droplets in an enzymatic network, Soft Matter, 14, 2018, 361.
10. Karina K. Nakashima, Alain A.M. André, and Evan Spruijt, Enzymatic control over coacervation, Methods in Enzymology, vol 646, Chapter 13, page 353, Elsevier, 2021
11. Shoupeng Cao, Lucas Caire da Silva, and Katharina Landfester, Light-Activated Membrane Transport in Polymeric Cell-Mimics, Angew. Chem. Int. Ed. 61, 2022, e202205266
12. Aman Agrawala, Jack F. Douglas, Matthew Tirrelle, and Alamgir Karim, Manipulation of coacervate droplets with an electric field, PNAS 119, 2022, e2203483119
13. Hanjin Seo and Hyomin Lee, Spatiotemporal control of signal-driven enzymatic reaction in artificial cell-like polymersomes, Nature Communications, 13, 2022, 5179
14. Dong Hyun Kim, Mi-Ran Ki, Da Yeon Chung, and Seung Pil Pack, Biomolecule-Based Coacervation: Mechanisms, Applications, and Future Perspectives in Biomedical and Biotechnological Fields, Biomolecules 15, 2025, 861
15. Karthika S Nair, Sreelakshmi Radhakrishnan, and Harsha Bajaj, Dynamic Duos: Coacervate-Lipid Membrane Interactions in Regulating Membrane Transformation and Condensate Size, Small, 21, 2025, 2501470
16. Shanta Biswas, Sai Venkatesh Pingali, Katie T. Tran, Qingqiu Huang, Xiaobing Zuo, and Amy Y. Xu, Mechanistic Insights into the Formation of Complex Coacervates in Crowded Environments, doi.org/10.1021/acs.biomac.6c01306
17. Ibraheem Alshareedah, Mahdi Muhammad Moosa, Matthew Pham, Davit A. Potoyan, and Priya R. Banerjee, Programmable viscoelasticity in protein-RNA condensates with disordered sticker-spacer polypeptides, Nature Communications 12, 2021, 6620.
18. Siddharth Deshpande, Frank Brandenburg, Anson Lau, Mart G. F. Last, Willem Kasper Spoelstra, Louis Reese, Sreekar Wunnava, Marileen Dogterom, and Cees Dekker, Spatiotemporal control of coacervate formation within liposomes, Nature Communications 10, 2019, 1800.
19. Charles E. Sing and Sarah L. Perry, Recent progress in the science of complex coacervation, Soft Matter 16, 2020, 2885.
20. Artem M. Rumyantsev, Nicholas E. Jackson, and Juan J. de Pablo, Polyelectrolyte Complex Coacervates: Recent Developments and New Frontiers, Ann. Rev. Conden. Matt. Phys., 12, 2021,155.
21. Murugappan Muthukumar, Fluctuations, structure, and size inside coacervates, Eur. Phys. J. E, 46, 2023,79.
22. Jonghoon Lee, Yuri O Popov, and Glenn H Fredrickson, Complex coacervation: a field theoretic simulation study of polyelectrolyte complexation, J Chem Phys, 128, 2008, 224908.
23. Scott P. O. Danielsen, James McCarty, Joan-Emma Shea, Kris T. Delaney, and Glenn H. Fredrickson, Molecular design of self-coacervation phenomena in block polyampholytes, PNAS, 116, 2019, 8224.
24. Anisha Shakya, Martin Girard, John T. King, and Monica Olvera de la Cruz, Role of Chain Flexibility in Asymmetric Polyelectrolyte Complexation in Salt Solutions, Macromolecules 53, 2020, 1258.
25. Shensheng Chen and Zhen-Gang Wang, Driving force and pathway in polyelectrolyte complex coacervation, PNAS, 119, 2022, e2209975119.
26. Shensheng Chen and Zhen-Gang Wang, Charge Asymmetry Suppresses Coarsening Dynamics in Polyelectrolyte Complex Coacervation, Phys. Rev. Lett. 131, 2023, 218201.
27. Angelika E. Neitzel, Yan N. Fang, Boyuan Yu, Artem M. Rumyantsev, Juan J. de Pablo, and Matthew V. Tirrell, Polyelectrolyte Complex Coacervation across a Broad Range of Charge Densities, Macromolecules 54, 2021, 6878.
28. Jiaxing Yuan and Hajime Tanaka, Network-forming phase separation of oppositely charges polyelectrolytes forming coacervates in a solvent, Nature Communications, 16, 2025, 1517.
29. Lennard Holschuh and Joachim Dzubiella, Reactive Brownian Dynamics of Chemically Fueled Droplets: Roles of Attraction and Deactivation Modes, J Phys Chem B, 129, 2025, 626.
30. Emiko Zumbro and Alfredo Alexander-Katz, Multivalent polymers can control phase boundary, dynamics, and organization of liquid-liquid phase separation, PLoS ONE 16, 2021, e0245405.

31. Léa Beaulès, Judith Miné-Hattab, Pierre Illien, and Vincent Dahirel, A Brownian dynamics study of liquid-liquid phase separation in multi-scale chromatin networks, https://arxiv.org/abs/2605.14516.
32. Mithun Radhakrishna, Kush Basu, Yalin Liu, Rasmia Shamsi, Sarah L. Perry, and Charles E. Sing, Molecular Connectivity and Correlation Effects on Polymer Coacervation, Macromolecules, 50, 2017, 3030.
33. Boyuan Yu, Heyi Liang, Artem M. Rumyantsev, and Juan J. de Pablo, Isotropic-to-Nematic Transition in Salt-Free Polyelectrolyte Coacervates from Coarse-Grained Simulations, Macromolecules, 55, 2022, 9627.
34. Li-Wei Chang, Tyler K. Lytle, Mithun Radhakrishna, Jason J. Madinya, Jon Vélez, Charles E. Sing, and Sarah L. Perry, Sequence and entropy-based control of complex coacervates, Nature Communications, 8, 2017, 1273.
35. Sai Vineeth Bobbili and Scott T. Milner, A simple simulation model for complex coacervates, Soft Matter, 17, 2021, 9181.
36. Yunqi Li, Tongfei Shi, Lijia An, and Qingrong Huang, Monte Carlo Simulation on Complex Formation of Proteins and Polysaccharides, J. Phys. Chem. B, 116, 2012, 3045.
37. Jie Xiao, Yunqi Li, and Qingrong Huang, Application of Monte Carlo simulation in addressing key issues of complex coacervation formed by polyelectrolytes and oppositely charged colloids, Advances in Colloid and Interface Science, 239, 2017, 31.
38. Katarzyna Cieślik-Boczula, Alpha-helix to beta-sheet transition in long-chain poly-l-lysine: Formation of alpha-helical fibrils by poly-l-lysine, Biochimie 137, June 2017, 106.
39. Imen Naassaoui and Adel Aschi, Evaluation of Properties and Structural Transitions of Poly-L-Lysine : Effects of pH and Temperature, Journal of Macromolecular Science, Part B 58, 2019, 673.
40. Biplab Bawali, Alokmay Datta, and Jayashree Saha, Investigating lipid bilayer self-assembly and formation of ripple phase: Insights from a coarse-grained implicit solvent model, AIP Advances 14, 2024, 015162.

Supplementary Files

This is a list of supplementary files associated with this preprint. Click to download.

- pLLjob65T0.5frac0.05att0.15final.xyz
- pLLjob62T4.0frac0.05att0.15final.xyz
- pLLjob61T2.0frac0.05att0.25final.xyz
- pLLjob64T1.0frac0.05att0.15final.xyz
- pLLjob66T0.5frac0.08att0.15final.xyz
- pLLjob71T0.5frac0.08att0.00final.xyz
- pLLjob60T3.0frac0.05att0.15final.xyz
- pLLjob67T0.5frac0.07att0.15final.xyz
- pLLjob68T0.5frac0.06att0.15final.xyz
- pLLjob70T0.5frac0.08att0.15final.xyz
- pLLjob69T0.5frac0.05att0.15final.xyz
- pLLjob63T5.0frac0.05att0.15final.xyz
- pLLonlystructuralsummary.csv
- NVTMonteCarlopLLATP.f95
- NVTMonteCarlopLLonly.f95
- pLLATPnATP0200neut020pctenergy.dat
- pLLATPnATP0360neut036pctenergy.dat
- pLLATPnATP0340neut034pctenergy.dat
- pLLATPnATP0400neut040pctenergy.dat
- pLLATPnATP0300neut030pctenergy.dat
- pLLATPnATP0460neut046pctenergy.dat
- pLLATPnATP0600neut060pctenergy.dat
- pLLATPnATP0420neut042pctenergy.dat
- pLLATPnATP0800neut080pctenergy.dat
- pLLATPnATP1500neut150pctenergy.dat
- pLLATPnATP0700neut070pctenergy.dat
- pLLATPnATP0440neut044pctenergy.dat
- pLLATPnATP0900neut090pctenergy.dat
- pLLATPnATP0500neut050pctenergy.dat
- pLLATPnATP1000neut100pctenergy.dat
- pLLATPnATP0480neut048pctenergy.dat

- pLLATPnATP0200neut020pctfinal.xyz
- pLLATPnATP0360neut036pctfinal.xyz
- pLLATPnATP0300neut030pctfinal.xyz
- pLLATPnATP0440neut044pctfinal.xyz
- pLLATPnATP0400neut040pctfinal.xyz
- pLLATPnATP0340neut034pctfinal.xyz
- pLLATPnATP0420neut042pctfinal.xyz
- pLLATPnATP0460neut046pctfinal.xyz
- pLLATPnATP0500neut050pctfinal.xyz
- pLLATPnATP0600neut060pctfinal.xyz
- pLLATPnATP0480neut048pctfinal.xyz
- pLLATPnATP0800neut080pctfinal.xyz
- pLLATPnATP0700neut070pctfinal.xyz
- pLLATPnATP0900neut090pctfinal.xyz
- pLLATPnATP1000neut100pctfinal.xyz
- pLLATPnATP1500neut150pctfinal.xyz
- ATPinitialconfigurationnATP0360neut036pct.dat
- ATPinitialconfigurationnATP0200neut020pct.dat
- ATPinitialconfigurationnATP0420neut042pct.dat
- ATPinitialconfigurationnATP0500neut050pct.dat
- ATPinitialconfigurationnATP0300neut030pct.dat
- ATPinitialconfigurationnATP0340neut034pct.dat
- ATPinitialconfigurationnATP0380neut038pct.dat
- ATPinitialconfigurationnATP0700neut070pct.dat
- ATPinitialconfigurationnATP0400neut040pct.dat
- ATPinitialconfigurationnATP0480neut048pct.dat
- ATPinitialconfigurationnATP0800neut080pct.dat
- ATPinitialconfigurationnATP0460neut046pct.dat
- ATPinitialconfigurationnATP0440neut044pct.dat
- ATPinitialconfigurationnATP0600neut060pct.dat
- ATPinitialconfigurationnATP0900neut090pct.dat
- ATPinitialconfigurationnATP1000neut100pct.dat
- pLLinitialconfigurationbox50.dat
- ATPinitialconfigurationnATP1500neut150pct.dat

- pLLATPnATP0340neut034pctinput.macro
- pLLATPnATP0600neut060pctinput.macro
- pLLATPnATP0480neut048pctinput.macro
- pLLATPnATP0440neut044pctinput.macro
- pLLATPnATP1000neut100pctinput.macro
- pLLATPnATP0500neut050pctinput.macro
- pLLATPnATP1500neut150pctinput.macro
- pLLATPnATP0420neut042pctinput.macro
- pLLATPnATP0460neut046pctinput.macro
- pLLATPnATP0900neut090pctinput.macro
- pLLATPnATP0200neut020pctinput.macro
- pLLATPnATP0300neut030pctinput.macro
- pLLATPnATP0360neut036pctinput.macro
- pLLATPnATP0380neut038pctinput.macro
- Energytable.csv
- ClusterVolumetable.csv
- ATPperChaintable.csv
- ATPDensitytable.csv
- NetChargetable.csv
- ClusterSizesummary.csv
- Reetable.csv
- PLLDensitytable.csv
- ClusterSizetable.csv
- RadialProfiletable.csv
- Summaryallorderparameters.csv